DYNAMIC INVESTIGATION OF THE PONTE TARO BRIDGE IN PARMA

Andrea Benedetti

Università degli Studi di Bologna
Dipartimento DICAM
Viale Risorgimento 2, 40136 Bologna, ITALY

Abstract

This paper presents the results of a systematic investigation of one of the oldest Italian masonry bridges. The Taro bridge, built 1826, underwent both static and dynamic testing aimed at checking the structural effectiveness. A non-destructive testing campaign was carried out in order to define the mechanical properties of bricks and mortar. Following the data acquisition, several finite element models were prepared allowing a careful interpretation of the observed behaviour. One of the most important parameter used to fit the data is the foundation compliance, which can be defined on the basis of geotechnical data. The comparison of the main frequencies obtained in a systematic scan of the 19 spans, pointed out one outlier frequency in the fifth span, where a consistent lack of the masonry arch texture was identified on the basis of the experimental campaign.

Keywords

masonry bridge, dynamic identification, frequency shift, damage detection, masonry properties

1 INTRODUCTION

In 1816 the Austrian duchess Marie Louise Habsburg Lorena dictated the construction of the bridge over the Taro River, dealing the project to the Italian engineer Antonio Cocconcelli, who was professor of hydraulics at the University of Parma.

The October 10th 1819 the duchess led the first stone of the bridge in the middle of an happy people crowd, granting a 250 liras dowry to 25 poor brides with a lottery. One ordinance issued by the duchess owed the mayors of the towns composing the dukedom to catch all the indigents capable to work and send them to the bridge construction site, where they received a good salary for the work, but all the escaping slackers were prisoned by the dragons and forced to join the works.

The great bridge was opened in October 1821 with a ceremony (see figure 1). The total cost of the bridge raised to 2,000,000 liras. Stamps and coins were drawn for this inauguration.

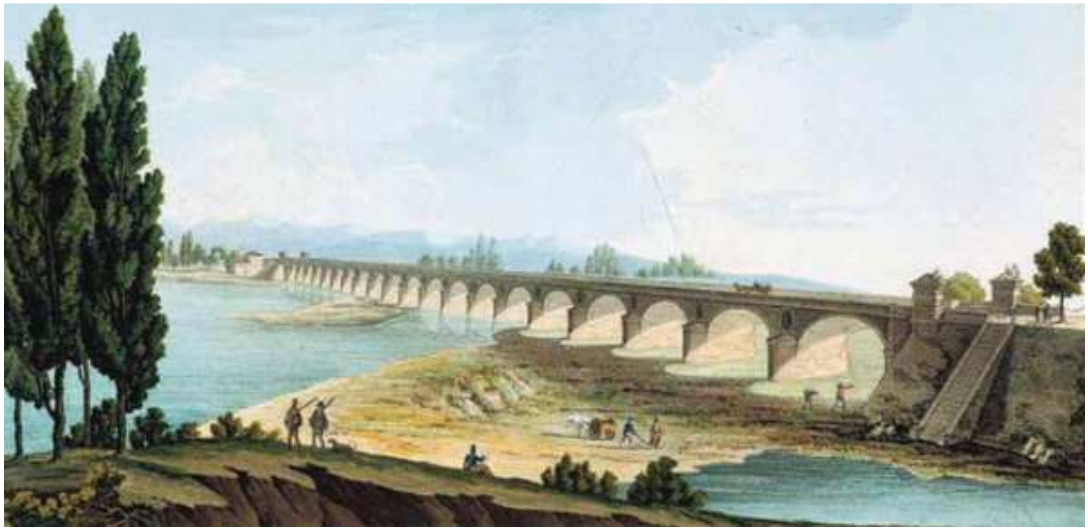

Figure 1 – Ponte Taro bridge, Anonymous, 1819, Glauco Lombardi Museum

Several maintenance works were completed in subsequent years, due to exceptional floods of the Taro River, and in these works the flooding holes were introduced in the bridge body (Cocconcelli, 1825). In 1828 after the completion of the restoration works, at the two entrance sections of the bridge, four marble statues were placed. The four sculptures of Giuseppe Carra represented the four Parma rivers: Parma, Taro, Enza and Stirone.

The taro bridge, composed of 20 spans for a total length of 565 m, connected from then on, in a fast way, the Emilia road founded by the romans.

A detailed information on the bridge features and the problems in the subsequent management and maintenance can be found in Cocconcelli (1825), and in recent historical analyses (Cornelli, 1958). In order to maximize the river flow, Cocconcelli designed the arches of the bridge according to Perronet's work (Perronet, 1792), by using polycentric circular curves that fit very well with elliptic curves. The construction of polycentric arches required well done scaffolds which are even discussed in detail in hydraulics books of that age (Cavalieri San Bartolo, 1833, see figure 2).

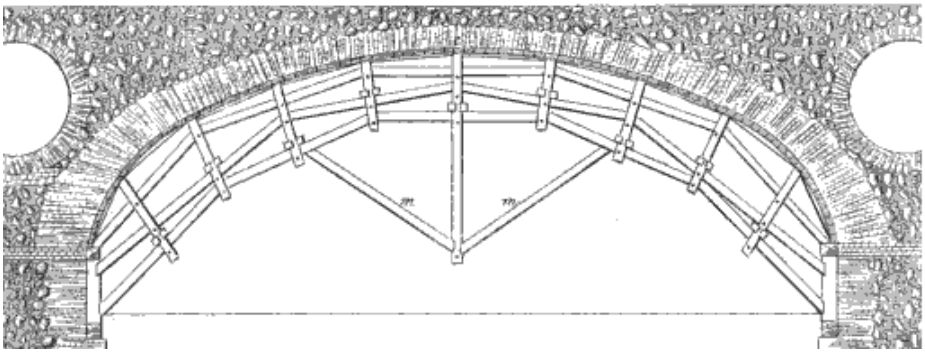

Figure 2 – Scaffolding proposed by Cavalieri San-Bartolo in the construction of a polycentric arch

The Taro bridge has many localized damages in the masonry structure and in the stones protecting the parapets and the edges of the flooding holes. Some brick textures are weathered by exposition to salt or river flooding, some mortar courses have been repeatedly repointed, and even the foundations have been stabilized by pouring concrete and cyclops stones around some piers. In the following some pictures of the damage evidences are presented (LGE, 2016, figures 3 and 4).

Figure 3 – View of the masonry damage in the spandrel wall

Figure 4 – View of the damaged masonry at the drainage pipe and on a stone corniche

2 GEOMETRICAL AND MECHANICAL RECONSTRUCTION OF THE BRIDGE

The bridge has a total width of 8.0 m and is composed of 20 spans of 28.0 m pier to pier distance; the arch span is 24 m and its sag 6.70 m. The arch line is composed of three circular segments of different opening and radius in order to produce a nearly elliptic geometry. The external arch segments have a radius of 4,7 m and an opening of 60°, while the central one has an opening of 60° but a radius of 19,7 m. In the following figure 5 one span of the bridge is shown in detail.

Figure 5 – Typical span of the Taro bridge

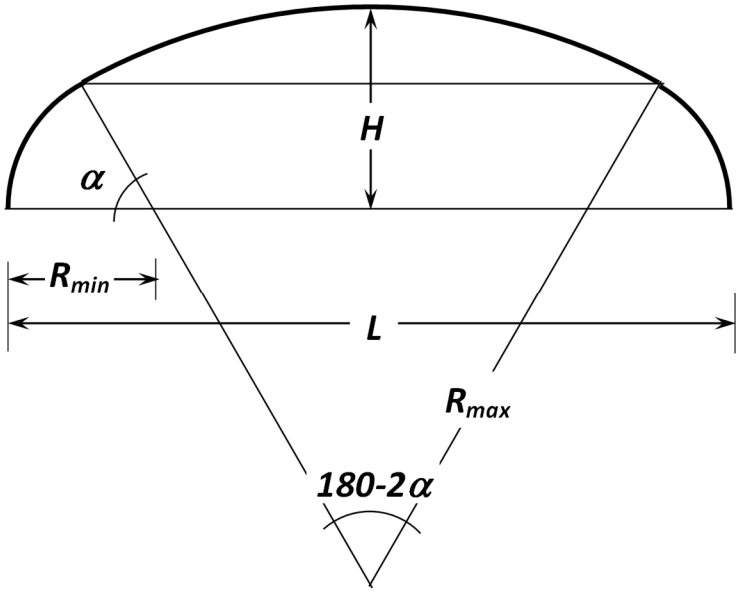

Figure 6 – Polycentric circle segments forming the Perronet Arch

The formulas that allow the construction of the arch are (figure 6):

$$\cos\alpha = \frac{L - 2R_{\min}}{2(R_{\max} - R_{\min})}\ ,\ \sin\alpha = \frac{R_{\max} - H}{R_{\max} - R_{\min}}\,, \qquad (1)$$

Where R_{min} and R_{max} are the arch radiuses, L the total span and H the total sag.
Other geometric details are the thickness of the arches, which run from 1.0 m at the crown

to 1.70 m at the supports, the diameter of the holes, which can be estimated as 4.0 m, and the thickness of the spandrel walls, which is of the order of 1.0 m too. Some critical parameters as the extension of the foundations and the soil stiffness have to be inferred from a back analysis of bridge tests, by using an identification procedure on a suitable numerical model.

A large part of the bridge body has undergone almost no modification in the masonry texture from the construction age, but several weathered arch volumes and stone edges are visible nowadays or have been restored in recent times. The most important rehabilitation work that is present in the masonry surface is the repeated repointing of the mortar courses with high strength mortar. This last intervention is certainly due to the progressive erosion of the original (weak) mortar due to the repeated river floods.

The mechanical characterization of the brick and mortar properties has been performed by using non-destructive testing (NDT) tools, as presented in Marastoni et Al. (2016), Marastoni et Al. (2017), Pelà et Al. (2016). In particular, the Torque Penetrometric Testing (TPT) was used for internal weak mortars, while the Helifix Pull out Test (HPT) was used for external strong mortars and for bricks. The TPT tool is a toothed nail with D_e = 9 mm, D_i = 7 mm and length 15 mm; the HPT helix is a tool with D_H = 6 mm and length L_H = 30 mm. The evaluation formulas are discussed in full detail in the cited papers and are reported here only for sake of completeness:

$$f_{c,HPT} = \frac{F}{\pi D_H L_H} \cdot \frac{1+k_t}{k_t} = \frac{F}{566} \cdot \frac{1+k_t}{k_t}, \tag{2}$$

$$f_{c,TPT} = f_{c,0} \left[\frac{m_v}{2\sqrt{k_A D_e \left(D_e^2 - D_i^2 \right)}} \right]^{\frac{2}{\alpha}} = \left[\frac{m_v}{251} \right]^{1.28}. \tag{3}$$

The k_t value is the ratio of the tensile strength to the compressive strength, and can be set to 0.125 for bricks and 0.25 for mortars. In the following table 1 are collected the results obtained on the piers from 3 to 5 on the Parma side.

Table 1 – Experimental mechanical data for the bridge materials

	Bricks		External Mortar		Internal Mortar	
	HPT [N]	f_{cb} [MPa]	***HPT*** [N]	f_{cme} [MPa]	***TPT*** [N]	f_{cmi} [MPa]
Pier 1	1100.0	17.49	687.5	6.07	459.9	2.17
Pier 2	1081.8	17.20	612.5	5.41	478.5	2.27
Pier 3	940.0	14.95	425.0	3.75	414.8	1.91
Mean	1040.6	16.5	575.0	5.1	451.1	2.1
COV	8%	8%	24%	24%	7%	9%

3 BRIDGE TESTING

The North third span of the bridge has been tested with static and dynamic loading, by recording displacements, velocities and accelerations (LGE, 2016). Figures 7 and 8 present

the positioning of the reference points for the deflection optical measurements and of the accelerometers and seismometers used for the dynamic investigation of the bridge.

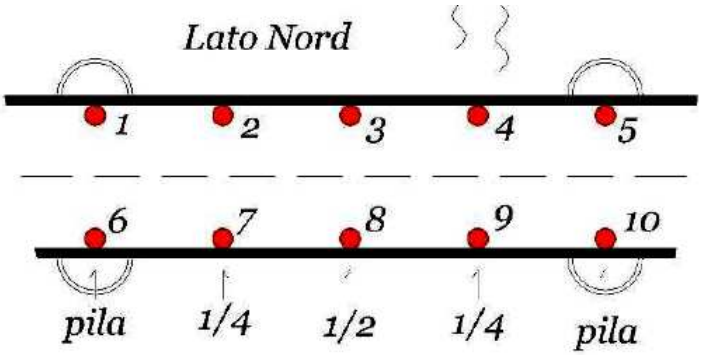

Figure 7 – Instrumented points for the static loading test

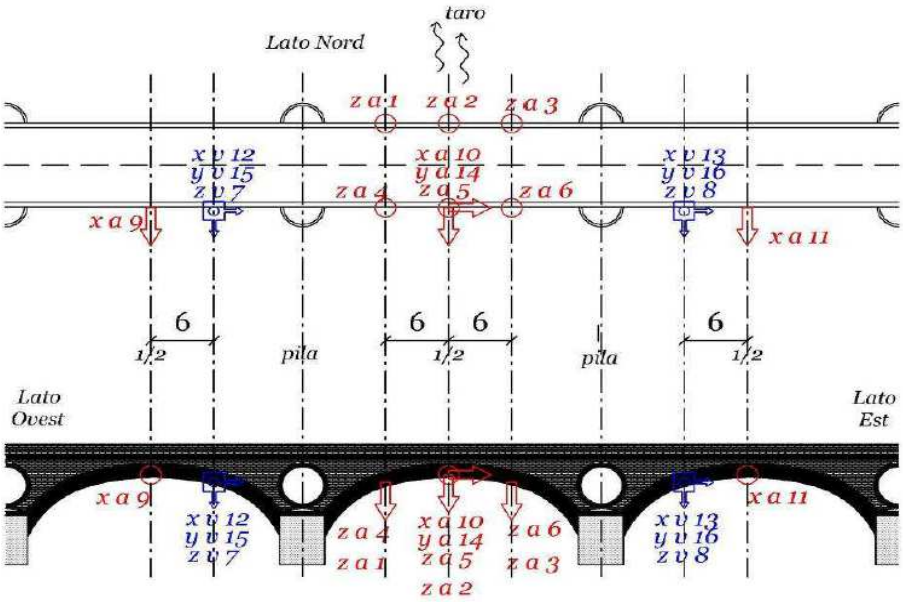

Figure 8 – Position of the accelerometers (a) and seismometers (v); the three indices x, y, and z point out the measurement directions (transversal, longitudinal, vertical)

3.1 Dynamic Investigation

The dynamic investigation was driven twice. Firstly, with reference to vibrations induced by moving loads, data were obtained by moving trucks of approximately 300 kN back and forth over the bridge. Then, the measurements were gathered by recording for three hours the accelerometer and seismometer signals under ordinary conditions. The subsequent FFT analysis allowed for the extraction of the main frequencies and the damping of the bridge. It is to consider that each span in a multi span continuous bridge has a slightly different dominant frequency due to the different restraint exerted by the remaining parts of the bridge itself. Theoretically, the spans symmetrically laying with respect to the central axis should show the same dominant frequency, so that in a total length perfect model, every frequency can appear twice due to symmetry.

The PSD of the recorded signals are presented in the following figures 9 and 10.

The PSD analysis and comparison gave the main results of table 2.

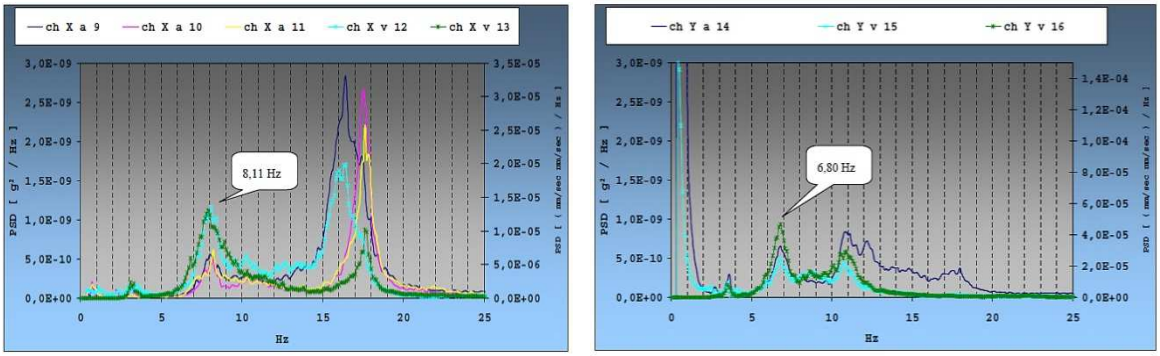

Figure 9 – PSD of the signals recorded in "x" transversal direction and in "y" longitudinal direction

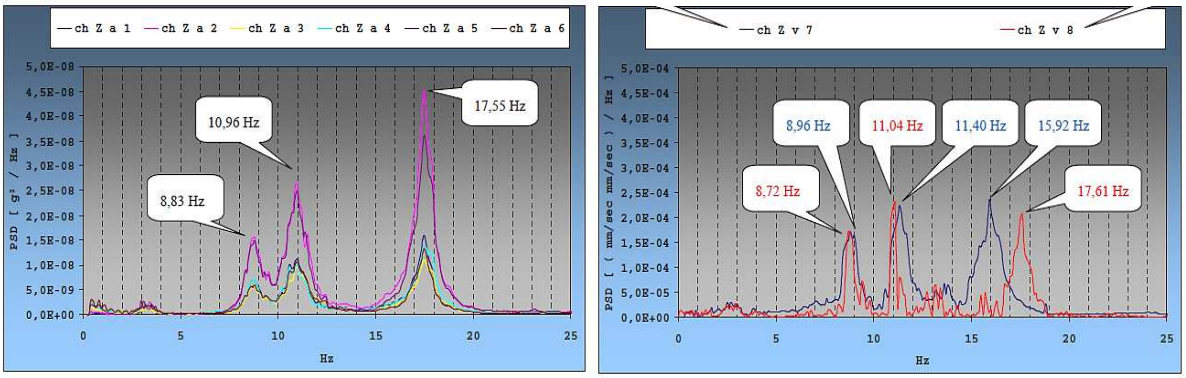

Figure 10 – PSD of the signals recorded in "z" vertical direction

Table 2 – Results of the dynamic identification

Mode	Mode Type	Direction	Frequency [Hz]	Damping [%]
1	extensional	Y	6.80	-
2	flexural	X	8.11	3.77
3	flexural	Z	8.83	3.47
4	flexural	Z	10.96	-
5	torsional	Z	17.55	1.38

3.2 Static loading

The static loading has been executed by using three different configurations of four full weight trucks, as depicted in the following figure 11. All the trucks weighted approximately 302 kN.

The displacements of the bridge characteristic points were measured on five equally spaced sections along the two parapet lines. This allowed the reconstruction of the deformed shape of the bridge at the top of the spandrel walls. The maximum recorded deflection was less than 1.0 mm for all the truck distribution schemes tested. In the following, the obtained settlement curves will be compared with the result of the numerical model derived from the dynamic identification.

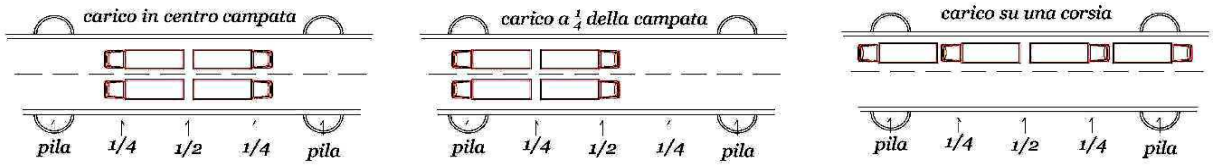

Fig. 11 – Truck arrangement for the static load testing of the bridge

Fig. 12 – View of the trucks over the bridge road for the static tests

4 MODEL IDENTIFICATION

On the basis of the experimental data of the masonry material and the dynamic tests of the bridge, a structural identification procedure was started, with the aim of defining a suitable finite element model able to interpret the observed behaviour.

In order to assess the feasibility of reduced FE models in the reconstruction of the structural features, three different models were prepared containing respectively three spans, six spans, and half of the bridge (figure 13).

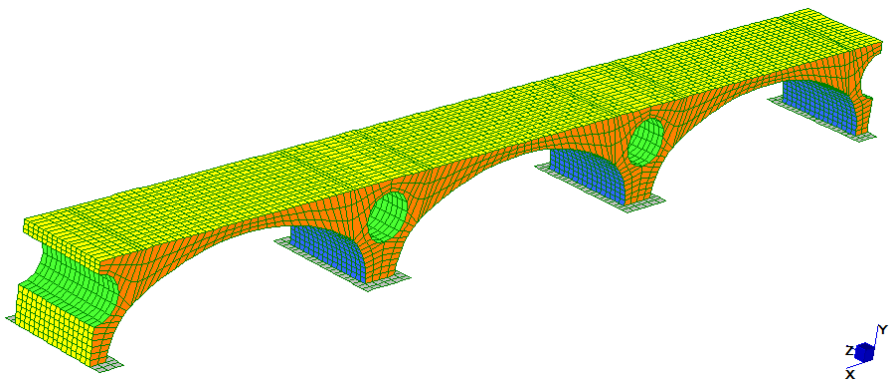

Figure 13.a – View of the model composed of three spans of the bridge (in yellow the fill)

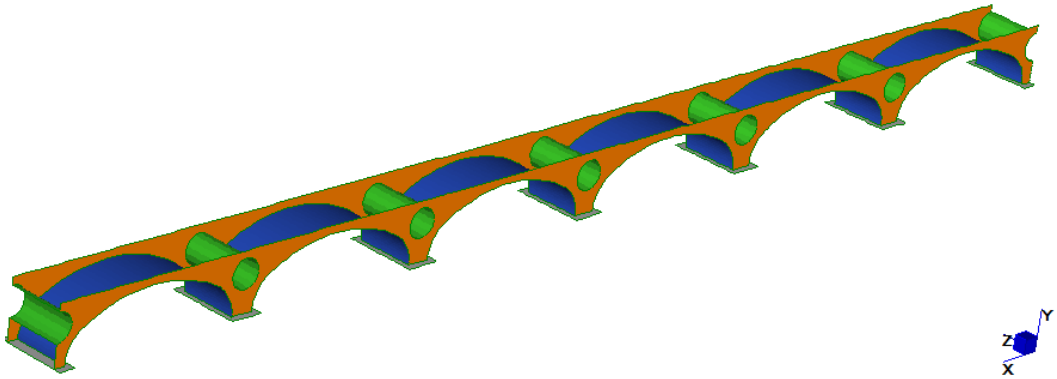

Figure 13.b – View of the model composed of six spans of the bridge (fill removed)

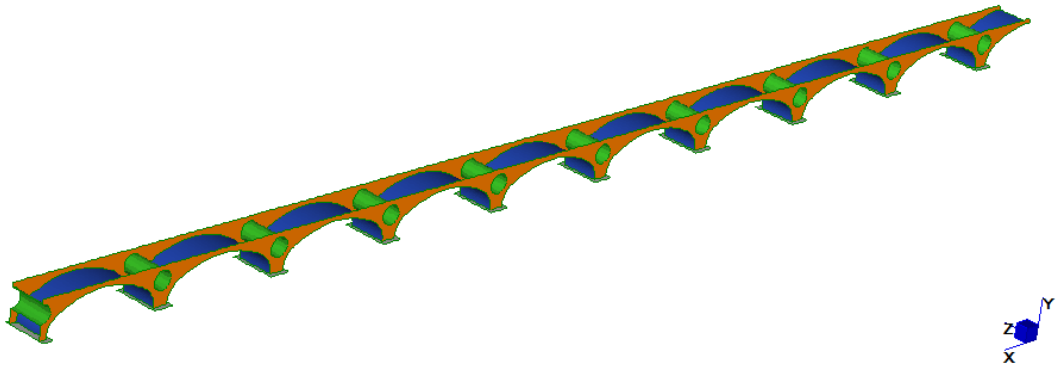

Figure 13.c – View of the model of half of the bridge (fill removed)

All the models are characterized by a hierarchy of the different composing parts. Namely, the arches, the pier external shells, the spandrel walls, the flooding holes and the parapets are modelled by using shell elements of given thickness, while the internal fill is modelled through solid prismatic elements, and the foundation blocks are introduced by a suitable spring bed representation based on a Winkler type soil behaviour.

The smallest model presents symmetry planes at both end sections, while the largest model presents a symmetry plane in the mid span of the bridge, and a fully fixed section on the abutment end. Since the extensional behaviour of the bridge along the axis is meant to be of very high frequency, the three model are able to show almost the same range of natural frequencies in vertical and transversal modes, even if the frequency set of larger model is certainly denser than the one of the reduced size model.

The main experimental parameter of the model is the elastic modulus of masonry elements, while the modulus of the fill and the soil reaction modulus can be adjusted by an identification procedure of the experimental frequencies.

The masonry modulus can be computed by using the compressive strength of bricks and mortars in evaluating the respective moduli, and finally by applying an homogenization procedure.

In table 3 the data of the materials composing the masonry walls are defined, together with their respective thicknesses and volume fractions. The masonry material properties are then derived accordingly to the following formulas:

$$E_j = \eta_j f_{cj}, \tag{4}$$

$$E_{M,i} = \left(t_b + t_{m,i}\right) \cdot \left(\frac{t_b}{E_b} + \frac{t_{m,i}}{E_{m,i}} \right), \tag{5}$$

$$E_{MH} = \alpha_1 E_{M,1} + \alpha_2 E_{M,2}\,, \tag{6}$$

$$f_{cM} = 0.6 \cdot f_{cb}^{0.7} \cdot \left(\alpha_1 f_{cm,1}^{0.3} + \alpha_2 f_{cm,2}^{0.3} \right), \tag{7}$$

In which the subscript M refers to masonry, b to bricks, and m,1 and m,2 to the two mortar types. By solving these formulas we obtain a masonry elastic modulus of 5300 MPa, and a masonry average strength of 5.95 MPa.

Table 3 – Properties of bricks and mortars

Property	Brick	Mortar 1	Mortar 2
f_c [MPa]	16.5	5.1	2.1
η [-]	500	700	900
E [MPa]	8273	3556	1905
t [mm]	55	15	15
α [-]	1	0.3	0.7

In conclusion, the adopted rounded properties are:

- **Arches**: thickness 1,5 m Elastic Modulus $5 \cdot 10^6$ kPa,
- **Spandrel Walls**: thickness 1,0 m Elastic Modulus $5 \cdot 10^6$ kPa,
- **Foundations**: thickness 2,0 m Reaction Modulus $1 \cdot 10^6$ kN/m^3,
- **Rubble Fill**: variable thickness Elastic Modulus $2.0 \cdot 10^6$ kPa.

All the materials have a specific mass of 1800 kg/m^3.

The fill elastic modulus and the soil reaction modulus are obtained by a best fit procedure with the experimentally recorded main frequencies. In the optimization process, a Latin hypercube trial and error procedure was used in the simplest three span model. In the following table 4 the numerical frequencies are compared to experimentally extracted ones. The main three natural modes of the identification model are shown in figure 14.

Table 4 – Comparison of the numerical frequencies with the experimental ones

Frequency	Mode Type	Experimental [Hz]	Numerical [Hz]
1	longitudinal	6.80	7.76
2	Transversal flexural	8.10	6.83
3	1° vertical mode	8.80	8.78
4	2° vertical mode		9.09
5	3° vertical mode	11.00	11.70
6	torsional	17.50	15.02

The convergence of the numerical and experimental results is noticeable even if only three

spans of the bridge were included in the model.

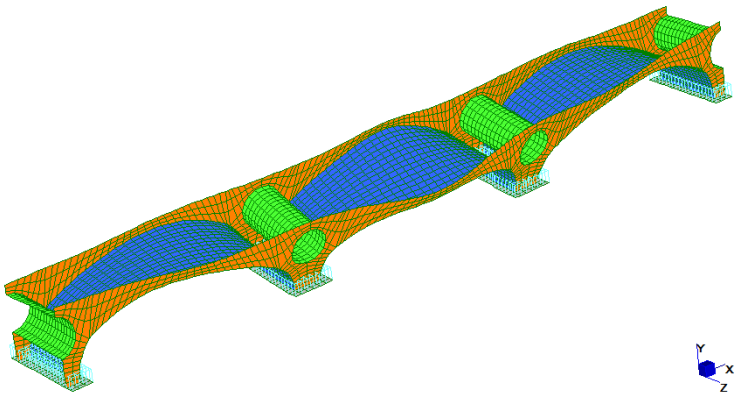

Figure 14.a – Transversal torsional-flexural mode, 6,82 Hz

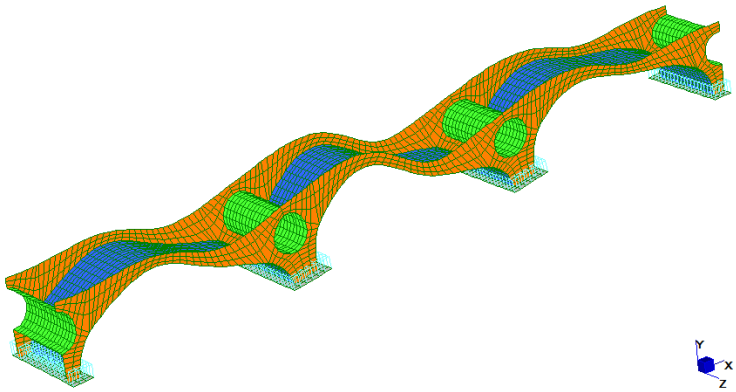

Figure 14.b – vertical flexural skew symmetric mode, 7,76 Hz

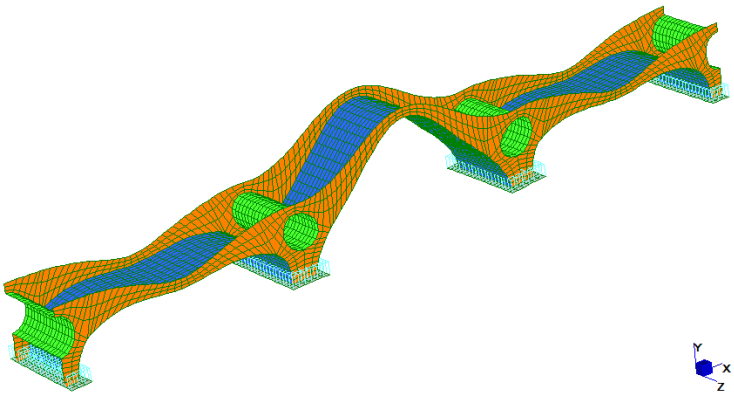

Figure 14.c – vertical flexural symmetric mode, 8,78 Hz

4.1 Evaluation of the static tests

As a check of the capability of the model in interpreting the bridge behaviour, the model has been employed in evaluating the results of the static loading tests (LGE, 2016, see figure 11). In particular, the used full loaded trucks were transformed in concentrated loads by using the schematic representation of the tire positions in table 5.

The bridge modes has been loaded with the three different truck composition schemes

shown in figure 11, namely on the crown, on the quarter span, on a lane. The obtained vertical displacements in the test were compared with the values obtained at the top of the spandrel walls. In the plots of figure 15 the numerical and experimental results of the three truck schemes are compared.

The comparison shows a very good agreement between the experimental and numerical values.

Table 5 – Load values and positions corresponding to a truck load

Variable	1° Axle	2° Axle	3° Axle	4° Axle
Abscissa [m]	1,1	2,5	4,6	6,0
Wheel Load [kN]	37,0	37,0	37,0	37,0
Clearance [m]	2,1	2,1	2,1	2,1

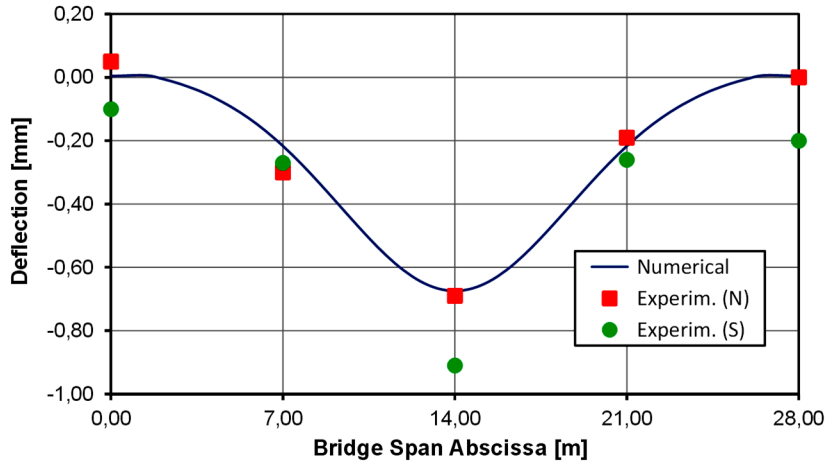

Figure 15.a – Deflection comparison for the crown loading (S = South lane, N = North lane)

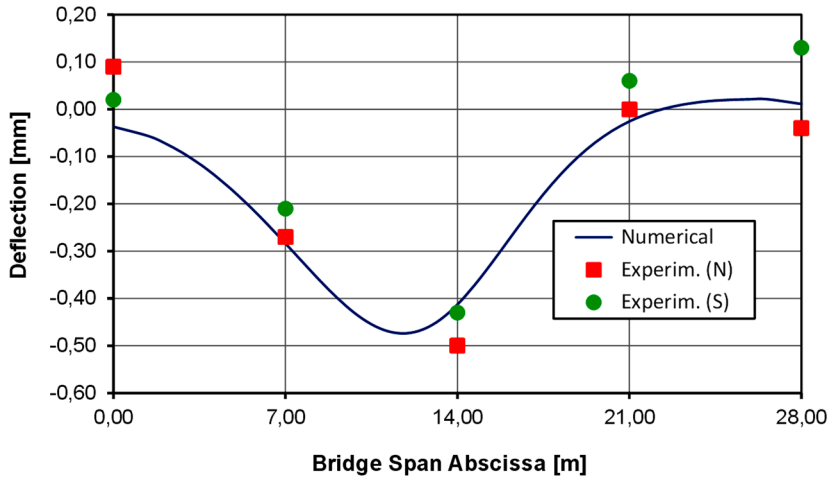

Figure 15.b – Deflection comparison for the loading at the arch quarter

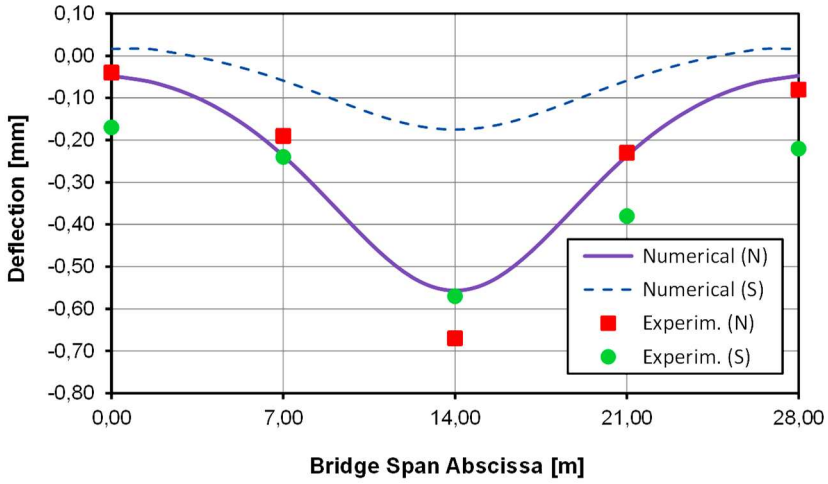

Figure 15.c – Deflection comparison for the line loading on one bridge lane

5 DYNAMIC COMPARISON OF THE 19 BRIDGE SPANS

After the static testing of the bridge, a careful investigation has been carried out with the SHAPE project in order to detect differences among the responses of the different spans composing the bridge. In particular, differences could be produced by different damage levels in the masonry textures, or by scour of some piers in the bridge. The 19th century bridges in Italy are in a consistent number (Re et Al., 2007), and they deserve special attention due to the increased environmental effects caused by the climatic change.

In what follows, the different spectra of the bridge span are presented and a comparison of a principal frequency outlined. The analysis of the signals is not very easy, since the various parts of the bridge introduce in the power spectra a number of secondary frequencies which can be difficult to separate (Nichols, 2013 and Tomor et Al., 2016).

Table 6 – comparison of the modes with higher participating mass

3 span model				6 span model				9.5 span model				9.5 span + parapets			
No.	Frequency	Mass	Mode	No.	Frequency	Mass	Mode	No.	Frequency	Mass	Mode	No.	Frequency	Mass	Mode
1	6.84	17.01	H	1	6.10	15.44	A	1	5.89	15.6	A	1	6.07	16.40	A
2	7.77	14.41	A	2	6.58	17.16	H	3	6.54	18.0	H	2	6.33	17.97	H
7	9.09	15.64	S	14	9.09	15.52	S	24	9.09	15.4	S	23	9.44	16.65	S
17	18.28	16.03	VS	35	18.29	15.90	S	58	18.30	16.4	S	58	18.45	15.59	S
	[Hz]	[%]	[-]		[Hz]	[%]	[-]		[Hz]	[%]	[-]		[Hz]	[%]	[-]

(TH = torsional – horizontal, VA = vertical antisymmetric, VS = vertical symmetric)

The comparison of the three models of different complexity reveals that by increasing the number of the spans, simply the number of the frequencies pertaining to each one of the frequency ranges increases, although the set of the ranges still remain unchanged, as is evident from figure 16 and table 6. This is due to the slightly different symmetric and

antisymmetric main frequencies of each span, when the effect of a variable number of neighboring spans is considered. However, as is evident in table 6, the modes with higher participating mass still point out almost the same principal frequency in all of the studied models.

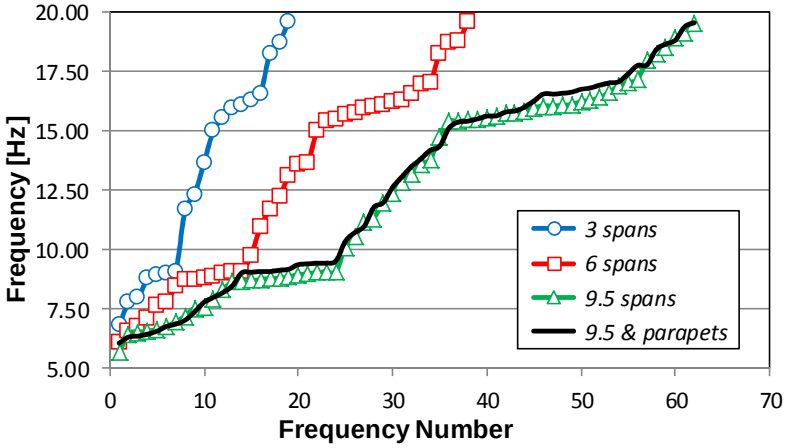

Figure 16 – Deflection comparison for the line loading on one line

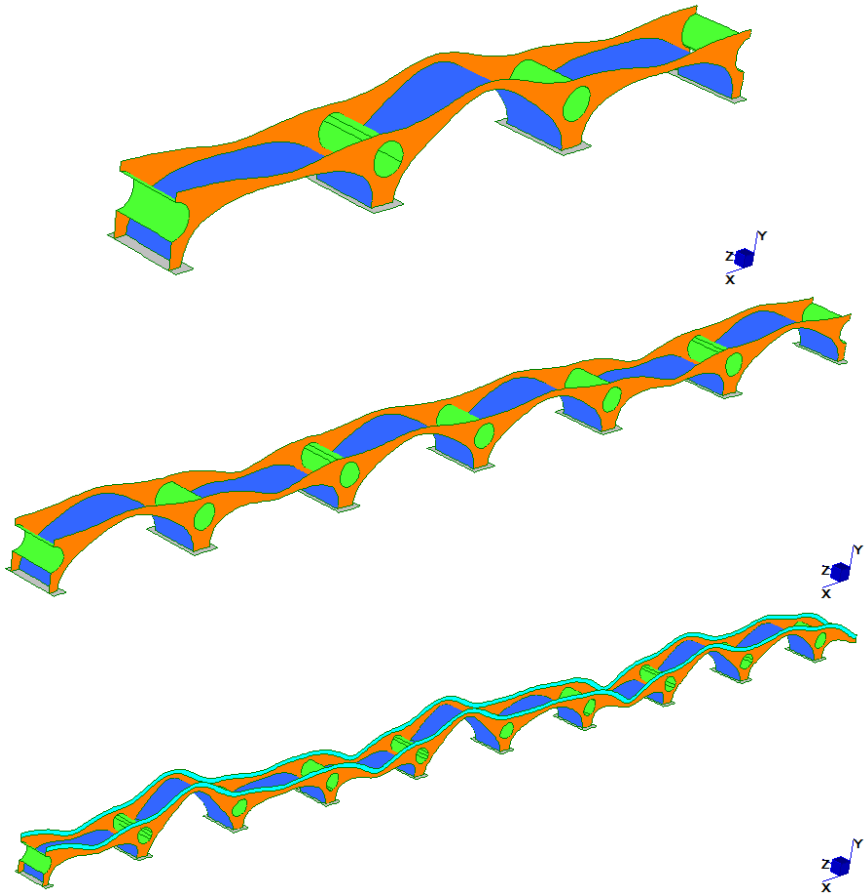

Figure 17 – The three modes with alternating hogging arches: 8.85 Hz approximately

Therefore it is possible to consider that if a span has a frequency lying outside a bounded range centered on the average frequency of all spans, this is a sensible indicator of local

damage in the span with frequency outliers.

A careful experimental campaign carried out on the bridge by recording the ambient traffic vibration on the two lanes of the 19 spans, pointed out that all the spans had frequencies remaining on a variation range set out as a +/- one standard deviation from the mean, apart the fifth span on the south side, which presented a definite anomalous shift (figure 18).

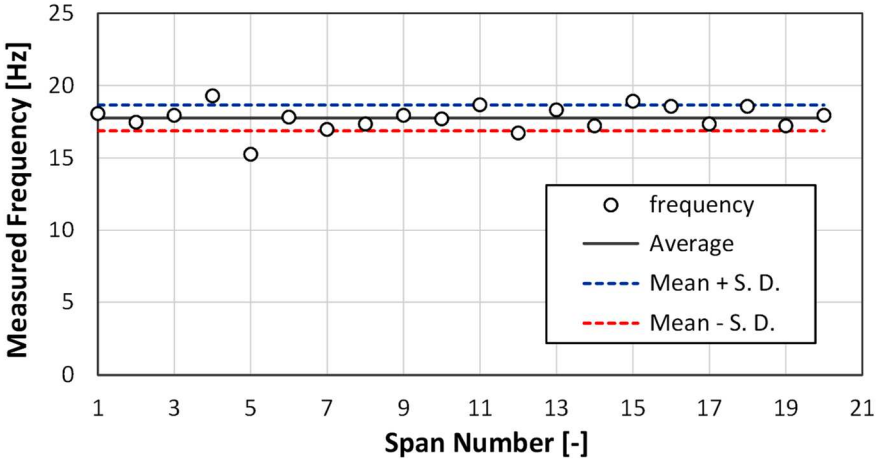

Figure 18 – Comparison of the selected frequency for the 20 bridge spans

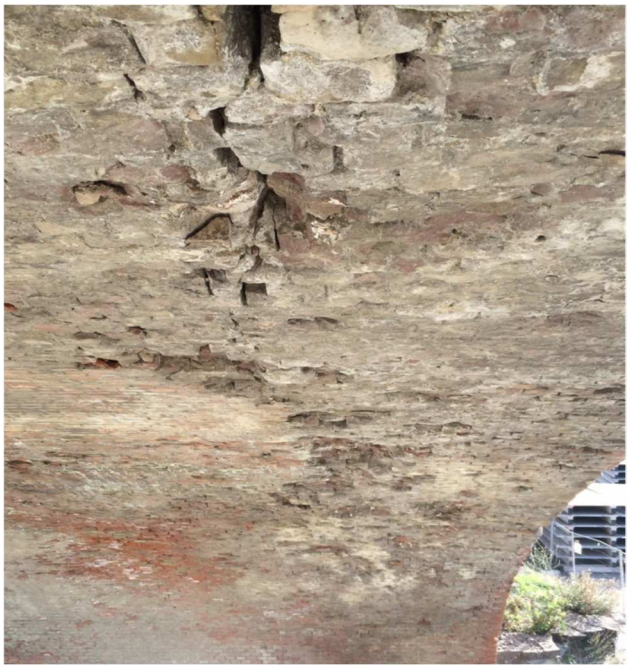

Figure 19 – View of the masonry damage and salt spread at the arch intrados

This frequency decay is linked with the damage detected in the lower face of the fifth arch, which is characterized by a huge crack. Since the arch probably has been repaired after the II World War, it is possible that the joining surface has opened during the subsequent use for reasons of cyclic loading or mortar deterioration caused by weathering.

It is evident that a planned schedule of frequency detection on masonry bridges can point out the efficiency level of the structure. A long path however still remains in front of us in

order to connect the information contained in the measurements with a real damage pattern deduction.

6 CONCLUSION

In the paper the 200 old Taro Bridge has been detailed in its geometrical and mechanical features. The bridge conditions show a diffused light damage state due to local deterioration of bricks and mortar.

The bridge was submitted to static and dynamic investigation and the results allowed preparing some numerical models which are capable to predict the observed behaviour. The comparison among the models pointed out that even a very short model of 3 spans is able to explain the dynamic features of the bridge.

Then, an episodic survey recorded the main frequencies of all the span composing the bridge. From this survey a slightly defective behaviour of one span was highlighted. A subsequent check on the bridge outlined the presence in the defective zone of an important crack running on the symmetry plane of the fifth span, which probably is the reason of the observed frequency shift.

The study points out several important features of the arch masonry bridges which renders this bridge class very peculiar and significant for the conservation of the structural heritage.

7 ACKNOWLEDGMENTS

This study has been partly granted by the EU through the ERA-NET Infravation 2014 research program, SHAPE project, Grant 31109806.004. The support of the Infravation program is gratefully acknowledged.

8 REFERENCES

[1] Cavalieri San-Bartolo N., (1833). *Istituzioni di architettura statica e grafica*. Firenze.

[2] Cocconcelli A., (1825). *Descrizione dei progetti e dei lavori per l'innalzamento dei due ponti sul Taro e sulla Trebbia.* Parma, Tipografia Ducale. (more information on Cocconcelli's work is present in https://it.wikipedia.org/wiki/Antonio_Cocconcelli)

[3] Cornelli B., (1958). Il ponte sul Taro e le amarezze dell'ing. A. C.. *Aurea Parma*, XLII, pp. 10-24.

[4] De Santis S., Tomor A.K., (2013). Laboratory and field studies on the use of acoustic emission for masonry bridges. *NDT & E International*, 55, pp. 64-74.

[5] LGE – Laboratorio Geotecnologico Emiliano, (2016). *Prove di Carico Statiche e Caratterizzazione Dinamica Su Porzione di Ponte Stradale*, Comunicazione Privata.

[6] Marastoni D., Pelà L., Benedetti A., Pignagnoli G., (2017). Torque Penetrometric Test for the in-situ characterisation of historical mortars: fracture mechanics interpretation and experimental validation. *Construction and Building Materials*, 157, pp. 509-520.

[7] Marastoni D., Pelà L., Benedetti A., Roca P., (2016). Combining Brazilian tests on masonry cores and double punch tests for the mechanical characterization of historical mortars. *Construction and Building Materials*, 112(1), pp. 112-127.

[8] Nichols J.M., (2013). A Modal Study of the Pont-Y-Prydd Bridge using the Variance Method. *Masonry International*, 26(2), pp. 23-33.

[9] Pelà L., Roca P., Benedetti A., (2016). Mechanical Characterization of Historical

Masonry by Core Drilling and Testing of Cylindrical Samples. *International Journal of Architectural Heritage*, 10(2-3). pp. 360-374.

[10] Perronet J.R., (1792). *Mémoire sur la recherche des moyens que l'on pourrait employer pour construire de grandes arches de pierre de deux cents, trois cents, quatre cents & jusqu'à cinq cents pieds d'ouverture qui seraient destinées à franchir de profondes vallées bordées de rochers escarpés*. Paris, Imprimerie Nationale du Louvre.

[11] Re L., Fantone M., De Vecchi B.V., (2007). Bridges of the Napoleonic roads in north-western Italy. *ARCH'07 – 5th International Conference on Arch Bridges*, Lourenço, Oliveira, Portela Ed.s. Madeira, Portugal.

[12] Tomor A., Nichols J.M., Benedetti A., (2016). Identifying The Condition of Masonry Arch Bridges Using CX1 Accelerometer. *ARCH 2016 Conference*, Wroclaw, Poland.

[13] UIC – International Union of Railways, (1995). Leaflet 778-3R, *Recommendations for the inspection, assessment and maintenance of masonry arch bridges*. Paris, UIC.